Mechanical and thermal stresses at shot particles during fatigue of Kaowool aluminum composites at 20°C

A. AL-OSTAZ
Composite Materials and Structures Center, 2100 Engineering Building, Michigan State University, East Lansing, MI 48824, USA

W. J. BAXTER
GM Research and Development Center, Warren, MI 48090-9055, USA

I. JASIUK
The G.W.W. School of Mechanical Engineering, Georgia Institute of Technology, Atlanta, GA 30332-0405, USA
E-mail: iwona.jasiuk@me.gatech.edu

During fatigue of Kaowool fiber reinforced aluminum composites at 20°C, cracks are initiated at hollow Kaowool particles. The stress concentrations associated with these particles arise from two sources: (i) residual stresses due to differential thermal contraction of the Kaowool and aluminum and (ii) the applied cyclic fatigue stress. These stresses are calculated from a finite element model which incorporates plasticity of the aluminum matrix. In general, the mechanical stresses are considerably larger than the thermal stresses. The total stress, in both the aluminum matrix and the Kaowool particle, increases with decreasing particle wall thickness and the proximity of the particle to the surface. In general, the stress concentrations in the aluminum matrix are more critical than those in the Kaowool particles, and are predicted to exceed locally the yield strength of 339 aluminum for all values of wall thickness. The particles observed experimentally at the fatigue fracture origins are thin walled and close to the surface, in quantitative agreement with the predictions of the finite element model.

1. Introduction

The tensile strength of Kaowool [1] fiber reinforced 339 aluminum composites equals the theoretical value for a perfectly bonded system over the temperature range from 20°C to 300°C [2]. But, the fatigue life at 300°C is limited by the presence of hollow thin walled Kaowool shot particles, which are typically spheroidal and act as sites for crack initiation [3]. An elastic analysis of the stresses associated with this type of defect at 300°C showed that the stress concentration factor (SCF) in the adjacent aluminum matrix increases substantially as the distance of the particle from the surface decreases, a relationship which is in excellent agreement with the particle geometries observed at the fatigue crack initiation sites [3]. More recently, we have performed a more accurate elastic plastic analysis of the role of particle wall thickness and shown that thin walled particles act as defects, while thick walled particles act as reinforcements, this transition being defined by a critical wall thickness [4].

This paper extends the previous stress analyses [3, 4] to simulate our fatigue experiments at room temperature (20°C). In this case it is necessary to include the residual stresses generated by differential thermal contraction of the Kaowool and aluminum, as the casting cools from its T5 heat treatment at 210°C. Since the total localized stress is the sum of the thermal (residual) stress and mechanical (applied) stress, the absolute values of the two stress components are required. To this end, the model is refined to include the effect of plasticity of the aluminum matrix.

2. Model

The finite element model of the shot particles is the same as that described previously [3]. Namely, to simplify the calculations (i) the 3D shot particle is represented by a 2D model, and (ii) a plane stress condition is assumed with the mechanical applied stress P in the x-direction and parallel to the surface (Fig. 1). The shot particle has an outside radius a, wall thickness t, and is located at a distance d from the surface of the composite. For a partial particle left at the surface after machining (Fig. 1b), its location is described by negative values of d, e.g. $d = -a$ corresponds to a hemispherical particle at the surface.

TABLE I Physical properties of Kaowool and aluminum

Property	Temperature (°C)	Kaowool	Aluminum
Young's Modulus (GPa)	20°C	120	75
	100°C	120	72
	170°C	120	70
	210°C	120	65
Poisson's Ratio	20–210°C	0.2	0.343
Thermal Expansion Coefficient (10^{-6}/°C)	20–210°C	5.4	21.7

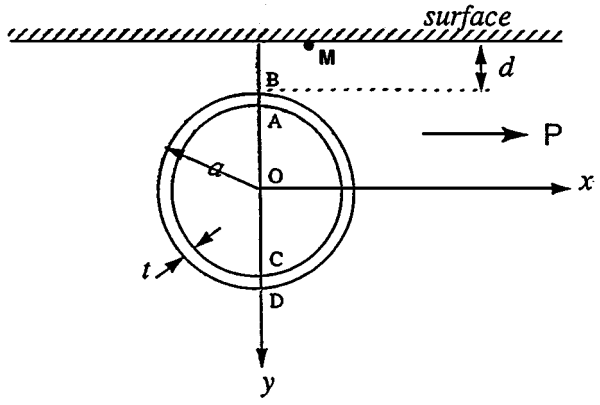

(a) Spherical particle beneath the surface

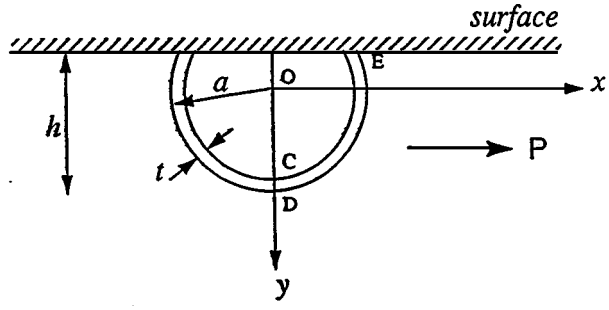

(b) Partial particle left at the surface after machining

Figure 1 Schematic diagram of model of hollow spherical shot particles: (a) particle beneath the surface, (b) partial shot particle left at surface after machining.

The stresses were calculated in the sequence in which they occur in practice. Firstly, the thermal stresses created by cooling the composite from 210°C to 20°C were simulated by a sequence of three discrete cooling steps: 210°C to 170°C, 170°C to 100°C and 100°C to 20°C, using the physical properties listed in Table I. For each step, the modulus and stress strain curve of the matrix was set equal to that of the unreinforced alloy (Fig. 2) at the lower terminating temperature (i.e. 170°C, 100°C and 20°C). Thus the distribution of thermal stresses at 170°C was the starting condition for the second cooling step, etc. Finally the thermal stress distribution at 20°C was the starting condition of the model for the application of a remote mechanical stress P parallel to the x-axis (Fig. 1). A value of $P = 120$ MPa was chosen, since a fully reversed axial stress of ± 120 MPa typically results in a fatigue life of 10^5 to 10^6 cycles for a 15% Kaowool/339 aluminum-T5 composite. Thus the

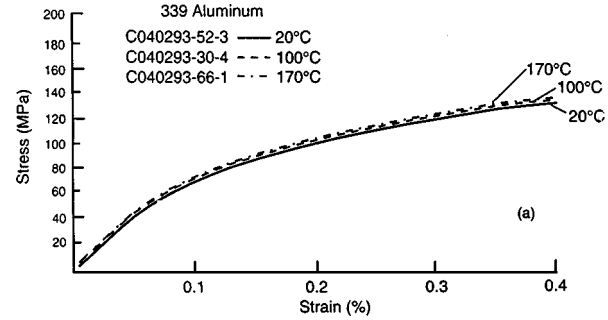

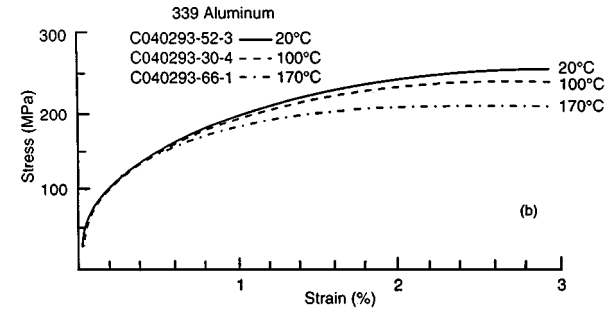

Figure 2 Stress strain curves for the unreinforced 339 aluminum matrix alloy at 20°C, 100°C and 170°C: (a) small strain region, (b) strained to failure.

TABLE II Tensile strengths (MPa) of Kaowool and 339 aluminum at 20°C

Tensile strength	Kaowool	339 Aluminum
Ultimate	1400	260
Yield (at 0.2% Strain)	—	124

final total stress distribution is the sum of the initial thermal stresses at 20°C and the mechanically induced stresses.

Since the aluminum matrix contracts more than the Kaowool, in general the thermal stresses in the matrix will be tensile while those in the Kaowool particle will be compressive. Thus for fully reversed loading ($R = -1$) as used in our experiments, the largest stress in the matrix is produced during the tensile loading, whereas the largest stress in the Kaowool occurs during the compressive loading. However, a brittle ceramic material such as Kaowool is undoubtedly much stronger in compression than tension. Therefore in our model only a tensile load is applied, as this is certainly the worst case scenario for the aluminum matrix and may also be so for the Kaowool.

The stresses presented in the following sections are restricted to specific locations of local maxima, such as A and C in the Kaowool shell, B and D in the aluminum matrix and M at the specimen surface (see Fig. 1). At these locations the quoted stress is σ_{xx}, since this component usually dominates. The significance of the values of total stress are judged from comparisons with the tensile strengths at 20°C of the 339 aluminum matrix and the Kaowool (Table II).

3. Shot particles remote from surface

When a shot particle is at a distance from the surface equal to twice the particle diameter, the stresses in the

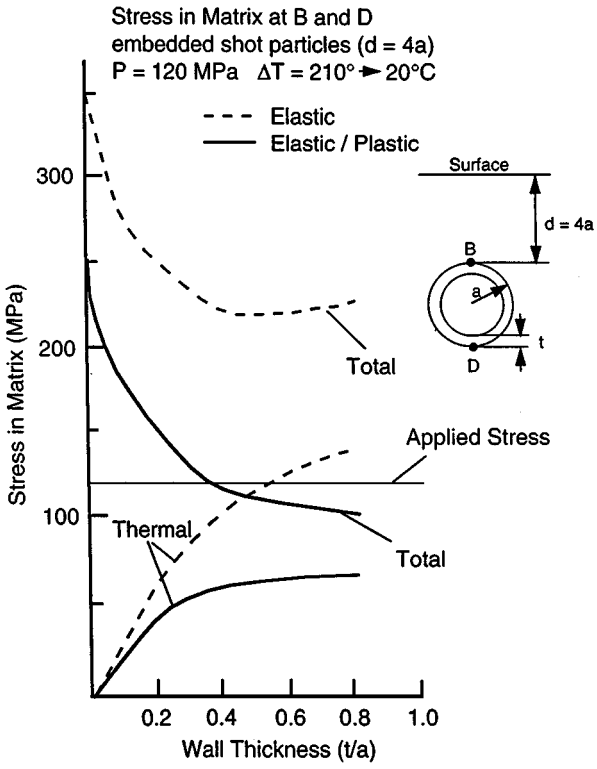

Figure 3 The effect of shot particle wall thickness on the thermal and total stresses in the aluminum matrix for totally embedded particles remote from the surface ($d = 4a$).

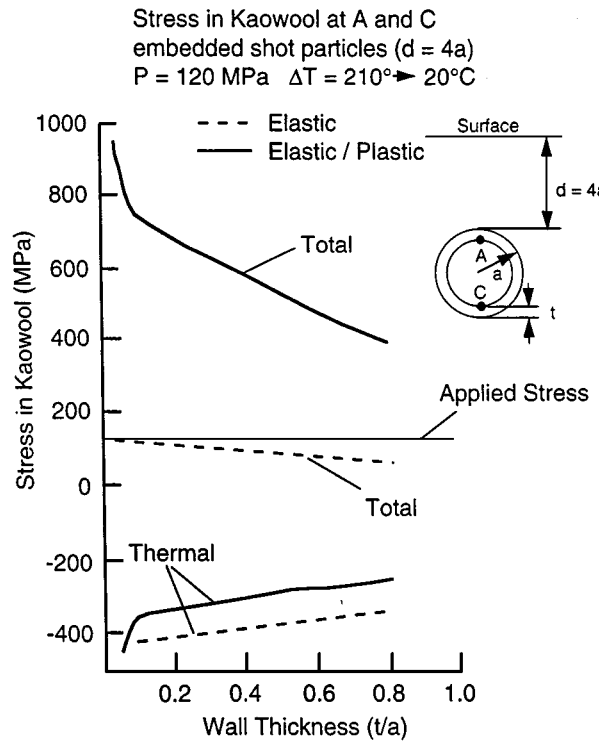

Figure 4 The effect of shot particle wall thickness on the thermal and total stresses in the Kaowool shell for totally embedded particles remote from the surface ($d = 4a$).

matrix at B and D are equal, i.e., there is no effect of the free surface and the particle behaves as if embedded in an infinite medium. The effect of shell wall thickness on these stresses is shown in Fig. 3, where the values for an elastic model are represented by the dashed curves, while the solid curves include the plasticity of the aluminum matrix. The thermal stresses increase with increasing wall thickness, whereas both the mechanical and total stresses decrease. (The mechanical stresses are not shown for simplicity.) As expected, the stresses for an elastic model are considerably larger than those obtained when plasticity is included. However, note that even for the elastic/plastic model, the total localized stress is larger than the applied stress for wall thicknesses $t < 0.38a$, i.e. these thin walled particles will act as defects. (This critical wall thickness would be only $0.18a$ in the absence of the thermal stress.)

Similarly, the stresses in the Kaowool shell at A and C are equal and are shown as a function of wall thickness in Fig. 4. Thermal stresses in the Kaowool are compressive while the mechanical stresses are tensile, and both decrease with increasing wall thickness. In the elastic model the thermal and mechanical stresses effectively cancel. Plasticity of the matrix transfers additional mechanical stress to the Kaowool so that the total stress is tensile and substantial for all wall thicknesses. Again, it is the thin walled particles which develop the largest total stresses.

Note that for thin walled particles with $t = 0.05$ to $0.1a$, which are typical of those found at crack initiation sites, the total stress in the Kaowool is considerably less than the tensile strength of Kaowool (1.4 GPa). In this situation the substantial compressive thermal stresses are very beneficial (Fig. 4). In the adjacent aluminum matrix (Fig. 3) the thermal stresses are small and contribute little to the total stress. Nevertheless, for $t < 0.37a$ the total localized stress in the matrix (Fig. 3) exceeds the tensile yield strength of the 339 aluminum (124 MPa).

4. Effect of proximity to the surface

As a thin walled particle approaches the surface, the stresses in the aluminum matrix at B and D are predicted to behave quite differently, as illustrated in Fig. 5 for $t = 0.05a$. At D, both the thermal and the mechanical components of the stress increase slightly as the particle approaches the surface. At B a very large increase of the thermal stress is accompanied by an even larger decrease of the mechanical stress so that the total stress also decreases. This marked reduction of the stress at B is compensated by the development of large tensile stresses on the surface at an off-axis location M, typically at a distance of 0.5 to 1.0a from the center line of the particle. (The thermal stresses at M are not significant so are not plotted in Fig. 5.) Therefore future discussion of the stresses in the matrix will focus on locations D and M.

The total stresses in the matrix decrease as the wall thickness of the particle increases: this trend is summarized for the two highly stressed locations D and M in Figs 6 and 7 respectively. The total localized stress at D is larger than the applied stress of 120 MPa for $t \leq 0.5a$, while the stress at M is larger than the applied stress even for $t = 0.8a$. Thus for all wall thicknesses considered here, when the shot particle is near the surface it is predicted to act as a defect.

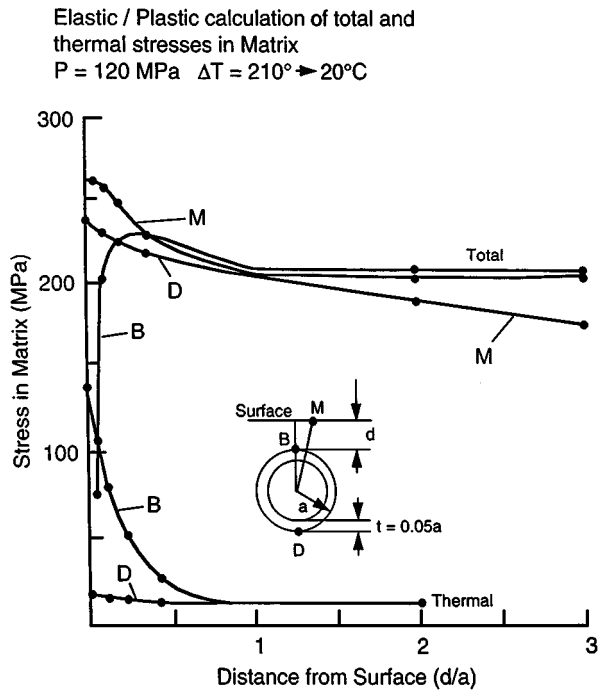

Figure 5 Effect of the distance of a shot particle from the free surface on the thermal stress at B and D and the total stress at B, D and M. $t = 0.05a$.

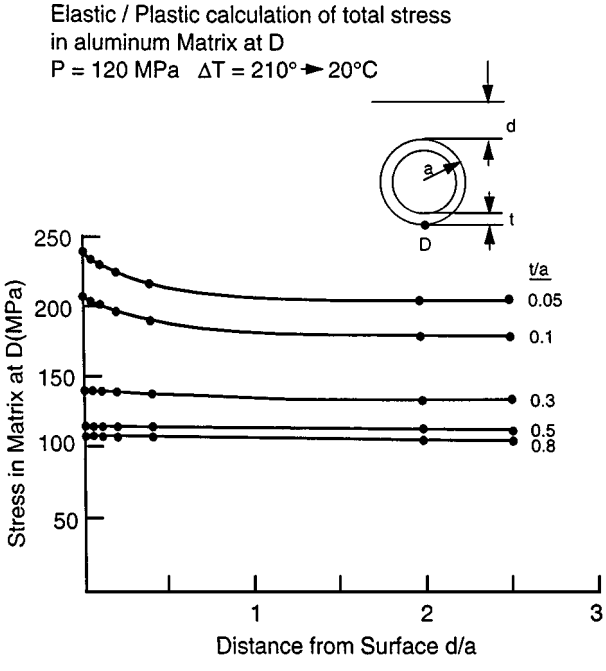

Figure 6 Effect of the distance of a shot particle from the free surface on the total stress in the aluminum matrix at D. The five curves correspond to five values of wall thickness as indicated.

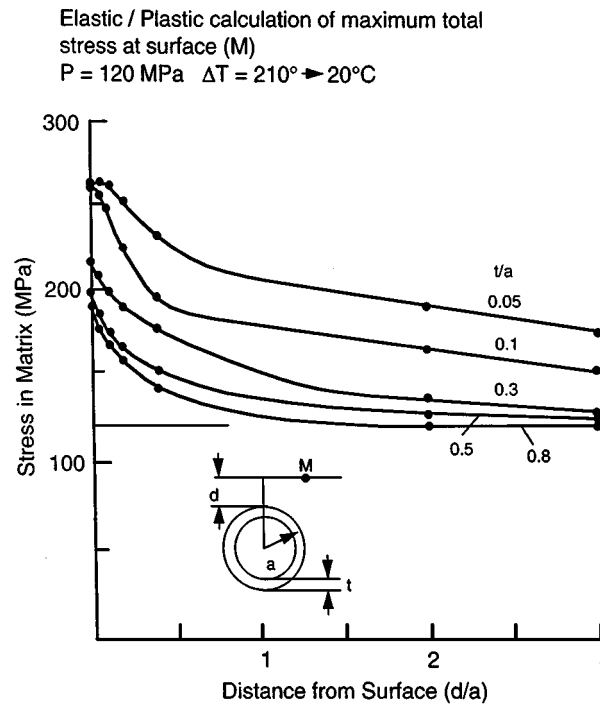

Figure 7 Effect of the distance of a shot particle from the surface on the maximum total stress at the surface at M. The five curves correspond to five values of wall thickness as indicated.

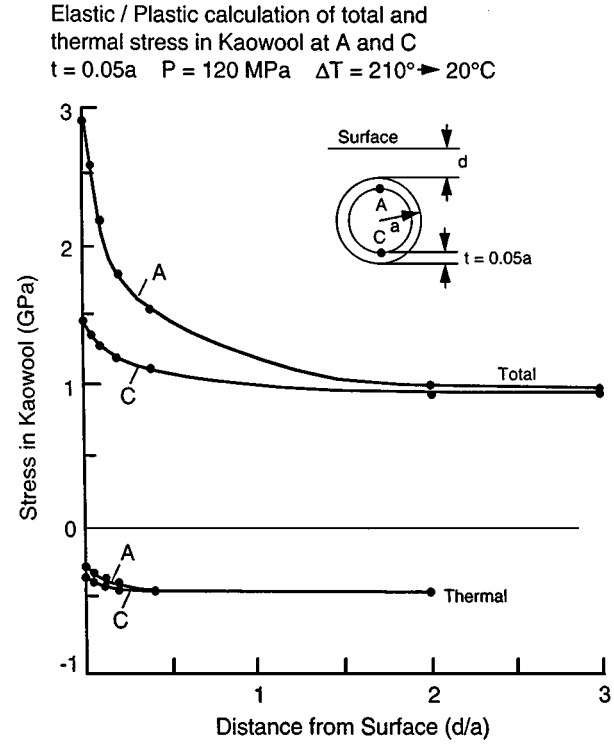

Figure 8 Effect of the distance of a shot particle from the surface on the total and thermal stresses in the Kaowool at A and C. Wall thickness $t = 0.05a$.

If the stress strain relationship for the matrix is changed to incorporate more work hardening and a higher ultimate tensile strength, the stress at D is increased, as expected. However, the stress at M is decreased while the stress at B no longer decreases as the particle nears the surface. Thus the appearance of a large stress at M, and the concomitant decrease of the stress at B, is accentuated by the development of plasticity around the shot particle.

The stresses in the Kaowool also increase as a particle approaches the surface, the stress at A increasing more rapidly than that at C (Fig. 8). These increases originate primarily from increases in the mechanical stresses, since the compressive thermal stresses only decrease by a small amount (Fig. 8). The increase in the total stress is very large only for thin walled particles, as is illustrated in Fig. 9 for location A. For $t = 0.05a$ and $0.1a$, the stress exceeds the tensile strength of Kaowool when the particle is near the surface.

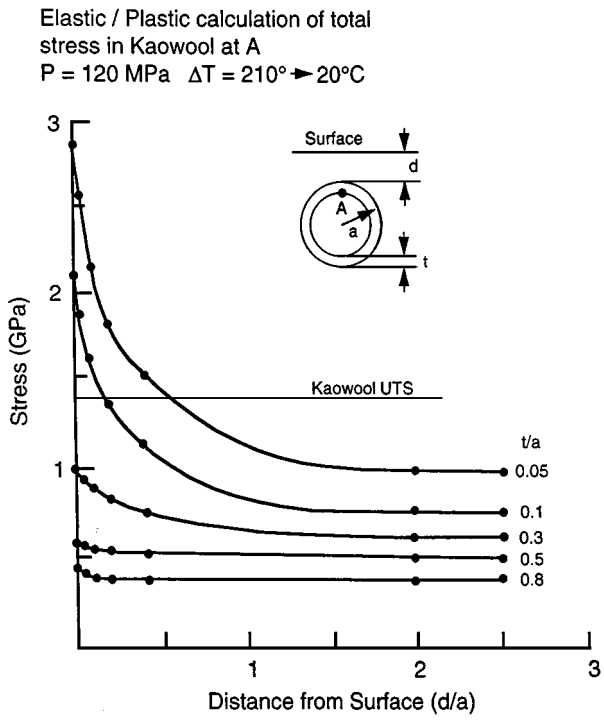

Figure 9 Effect of the distance of a shot particle from the surface on the total stresses in the Kaowool shell at A. The five curves correspond to five values of wall thickness as indicated.

5. Partial shot at surface

During machining, portions of shot particles may be removed leaving partial hollow shot particles exposed at the surface. In this situation the stresses will depend upon the fraction of particle remaining. This is illustrated in Figs 10 and 11 for particles with a wall

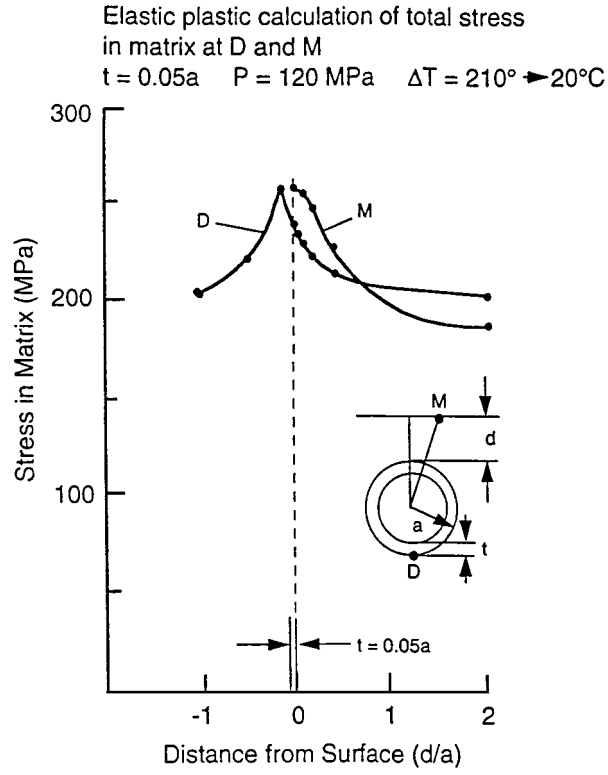

Figure 10 The total stress in the aluminum matrix at D and M for a shot particle with wall thickness $t = 0.05a$. The effect of distance from the surface encompasses embedded particles remote from the surface and fractional particles which remain after machining.

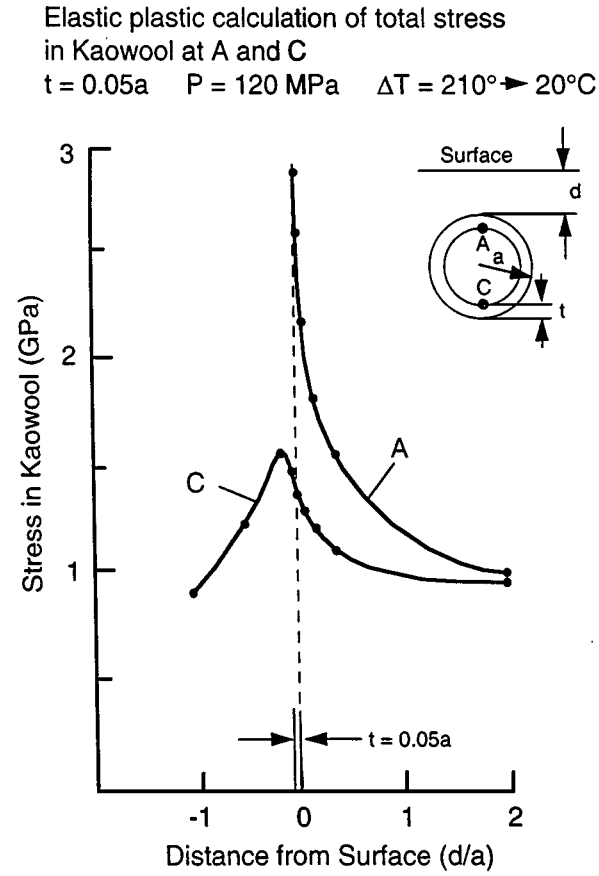

Figure 11 The total stress in the Kaowool at A and C for a shot particle with wall thickness $t = 0.05a$. The effect of distance from the surface encompasses fully embedded particles and the fractional particles which remain after machining.

thickness of $t = 0.05a$; the total stresses in the matrix at D and M are shown in Fig. 10, while those in the Kaowool at A and C are plotted in Fig. 11. The thermal stresses alone are not shown because they are not significant in comparison to the mechanical stresses. When a small portion of the particle has been removed ($d = -0.15a$), creating a small hole in the Kaowool shell, the localized stress in the matrix at D attains a maximum of 259 MPa. This value, which corresponds to the ultimate tensile strength of the matrix alloy at 20°C (Fig. 2), is also attained on the surface at M when the particle is very close to the surface, i.e. $d < 0.1a$. Similarly, the stress in the Kaowool at C attains a maximum value of 1.55 GPa when $d = -0.15a$, but the largest stress (2.9 GPa) occurs at A when the particle is at the surface, i.e. $d = 0$. Both these values exceed the ultimate tensile strength of Kaowool (1.4 GPa).

6. Effect of wall thickness

A convenient summary of the above results is provided by comparing an embedded particle (i.e. $d = 2a$) with those at or near the surface. Such a comparison is provided in Fig. 12, which shows the total stress in the matrix at D as a function of wall thickness; the curves correspond to $d = 2a$, $d = 0.2a$, $d = 0$ and the maximum stress produced when a particle has been partially removed by machining. When $t \leq 0.42a$, the stresses at D are larger than the applied stress regardless of their

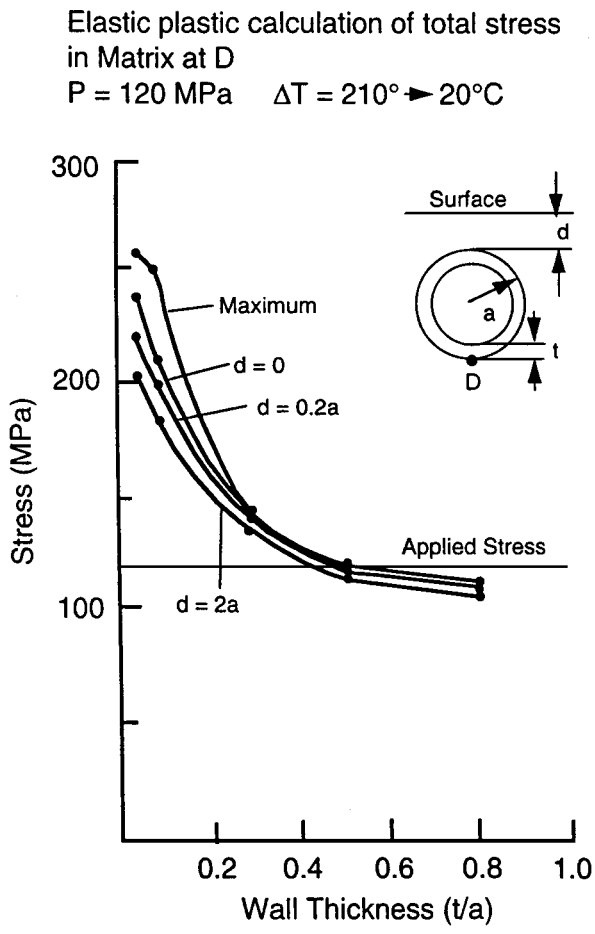

Figure 12 Effect of wall thickness on the total stress in the aluminum matrix at D. The four curves correspond to a particle remote from the surface ($d = 2a$), near the surface ($d = 0.2a$), at the surface ($d = 0$), and the condition of maximum stress when a small portion of the particle has been removed by machining.

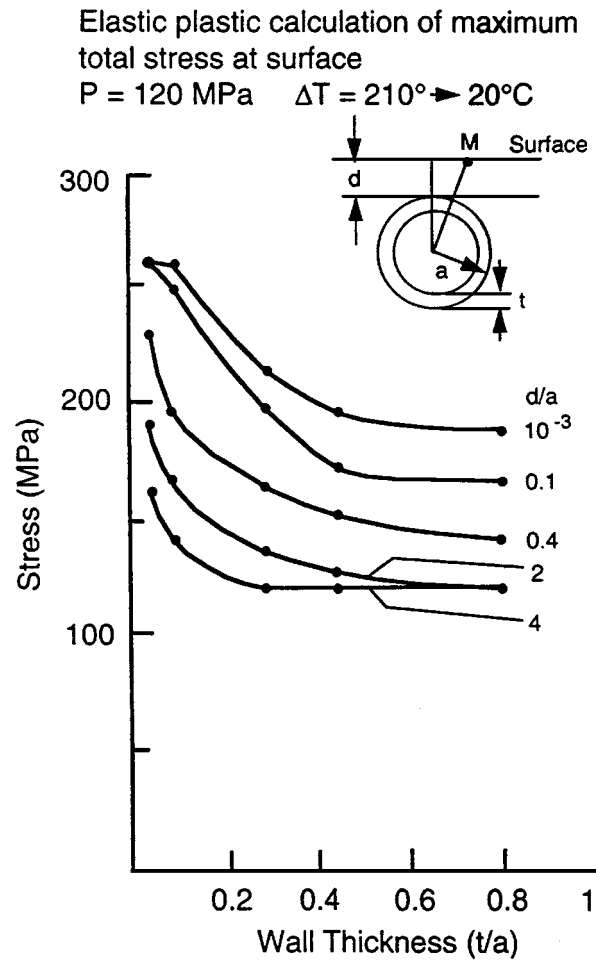

Figure 13 The effect of wall thickness on the total stress in the aluminum matrix at M for shot particles at various distances from the surface.

location, i.e. all these particles will act as defects. When a particle is at the surface ($d = 0$) the critical wall thickness increases to $0.47a$, while a partial particle will act as a defect if $t \leq 0.53a$.

The calculated total stresses at M are even more dire (Fig. 13): when the particle is near the surface (e.g. $d/a = 0.4$) the stress is larger than the applied stress for all values of wall thickness. The significance of this result will be discussed later. For the present, it suffices to note that the most devastating particles will be those with thin walls at or near the surface; under these conditions the calculated total stresses at both D and M approach the ultimate tensile strength of the 339 aluminum matrix.

A similar comparison of the total stresses in the Kaowool shell at A and C is shown in Fig. 14, where the curves for A correspond to $d = 2a$ and $d = 0$, while the one for C is the maximum stress attained for a partial shot particle at the surface. The stresses of primary concern are those which exceed the tensile strength of Kaowool. This occurs at A when $d = 0$ and $t < 0.2a$, and at C when $t < 0.06a$ and a small portion of the particle has been removed by machining. Again the critical particles are those with thin walls at or near the surface.

7. Comparison with fatigue failures

The fracture surfaces of eight specimens fatigue tested at 20°C were examined by scanning electron microscopy, and hollow shot particles were found at the crack initiation sites. The wall thicknesses ranged from $t = 0.05a$ to $t = 0.2a$ and their locations with respect to the surface are summarized by the histogram in Figs 15 and 16. Superimposed on this histogram is the calculated total stress in the matrix at D and M (Fig. 15), and in the Kaowool at A and C (Fig. 16), for shot particles with $t = 0.05a$ and $t = 0.1a$. Despite the small number of fatigue tests, the correlation is already quite good, with six of the eight crack initiating shot particles being close to the surface, where the calculated stresses are maximized.

The two specimens indicated by asterisks in Fig. 15 were examined in more detail and found to have several shot particles on the fracture surface. In one specimen, reinforced with 7% Kaowool, the crack initiated at the thin walled subsurface shot particle shown in the scanning electron micrograph in Fig. 17a. Of the other particles in the same sample, the two illustrated in Fig. 17b and c were judged to be the most significant from the viewpoint of the above stress analysis. The important geometrical parameters of these three particles are listed in Table III, together with the calculated total stresses in the matrix at D and M and in the Kaowool shell at A and C. It is significant that the largest stress, in both the aluminum matrix and the Kaowool shell, is associated with the particle at the fracture origin (Fig. 17a).

TABLE III Characteristics of the shot particles illustrated in Fig. 17 and the calculated stresses

Specimen: C100292-68-2 7% Kaowool/339 Al-T5
Fatigue Life: 2×10^6 cycles at ±124 MPa

Shot Particle	Wall Thickness (t/a)	Distance from Surface (d/a)	Calculated Stresses (MPa)			
			Matrix at		Kaowool at	
			D	M	A	C
Fracture Origin Fig. 17a	.05	1.74	204	192	1000	960
Fig. 17b	0.1	−1	187	—	—	740
Fig. 17c	0.1	4	188	165	791	762

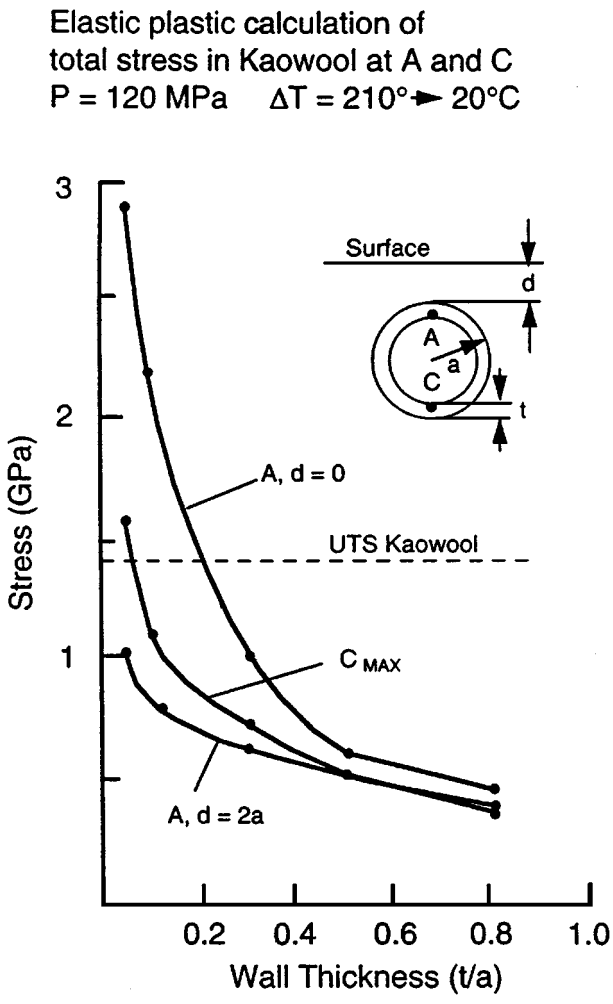

Figure 14 The effect of wall thickness on the total stress in the Kaowool at A and C. The bottom curve corresponds to particles remote from the surface ($d = 2a$), the top curve is for particles at the surface ($d = 0$). The middle curve is the maximum value of the stress at C attained when a small portion of the particle has been removed by machining.

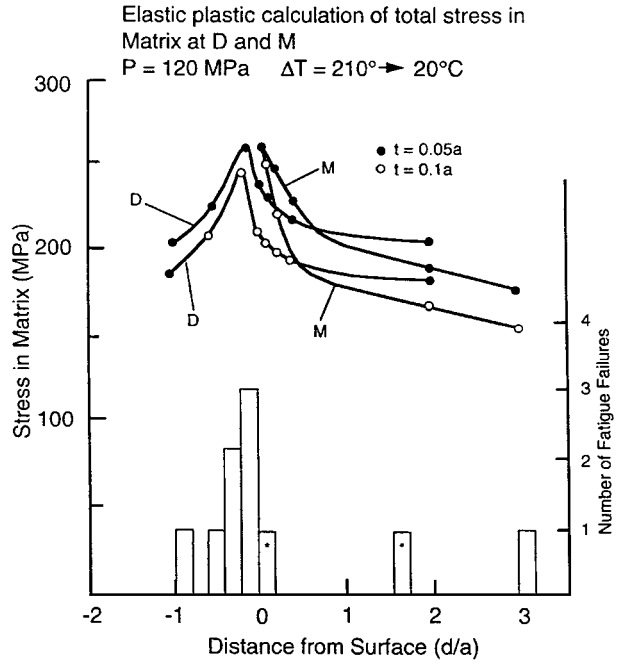

Figure 15 The total stress in the aluminum matrix at locations D and M for partial and complete shot particles as a function of their distance from the surface. The wall thicknesses $t = 0.05a$ and $t = 0.1a$ are typical of the particles causing fatigue failures. Superimposed is a histogram of the locations of the particles observed at the fracture origin of eight fatigue specimens. The two labeled with an asterisk are shown below in Figs 17a and 18b.

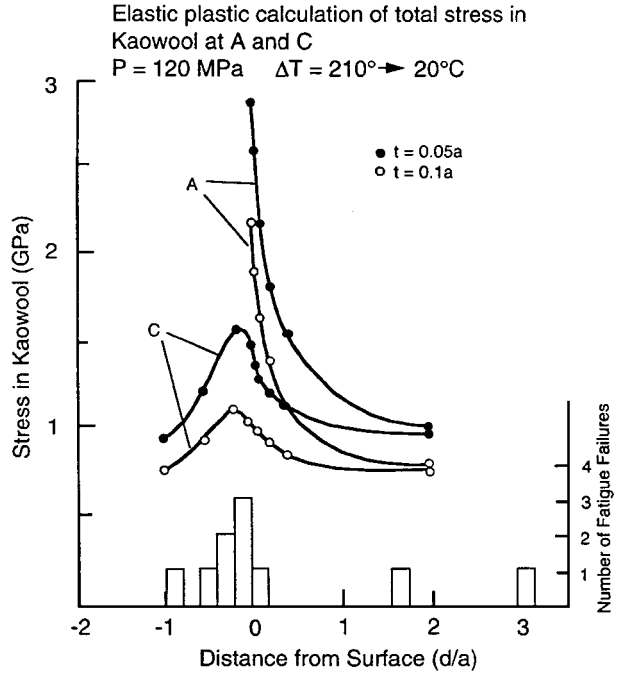

Figure 16 The total stress in the Kaowool shell at A and C for partial and complete shot particles as a function of their distance from the surface. The wall thicknesses $t = 0.05a$ and $t = 0.1a$ are typical of the particles causing fatigue failures. Superimposed is a histogram of the locations of the particles observed at the fracture origin of eight fatigue specimens.

In the second specimen, reinforced with 15% Kaowool, the fatigue crack initiated from a shot particle adjacent to the surface, as shown in the scanning electron micrograph in Fig. 18a. All of the other particles were much further from the surface; two of those closest to the surface are shown in the micrographs in Fig. 18b and c. The important geometrical parameters for all three particles, together with their calculated total stresses in the matrix at D and M and in the Kaowool shell at A and C, are summarized in Table IV. Again the largest stress, in both the aluminum matrix and the Kaowool shell, is associated with the particle at the fracture origin (Fig. 18a).

These two specimens also provide an interesting comparison in that, although they were fatigue tested at

TABLE IV Characteristics of the shot particles illustrated in Fig. 18 and the calculated stresses

Specimen: C051294-53-1 15% Kaowool/339 Al-T5
Fatigue Life: 1.85×10^5 cycles at ± 124 MPa

Shot Particle	Wall Thickness (t/a)	Distance from Surface (d/a)	Calculated Stresses (MPa)			
			Matrix at		Kaowool at	
			D	M	A	C
Fracture Origin Fig. 18a	0 .11	0.08	205	255	2100	1000
Fig. 18b	0.09	3	185	154	820	760
Fig. 18c	0.12	1.4	177	166	770	760

the same cyclic stress of ± 124 MPa, the 15% Kaowool specimen had a fatigue life (1.85×10^5 cycles) shorter than that of the 7% Kaowool specimen (2×10^6 cycles). This can now be understood in terms of the localized stresses calculated from our model (Tables III and IV). The maximum stresses, in the matrix at M and in the Kaowool at A, associated with the particle at the fracture origin in the 15% Kaowool specimen are substantially larger than those in the 7% Kaowool specimen.

More informative is a graphical representation of the largest stress associated with each of the six shot particles shown in Figs 17 and 18. The largest stresses in the aluminum matrix are plotted in Fig. 19, where they are

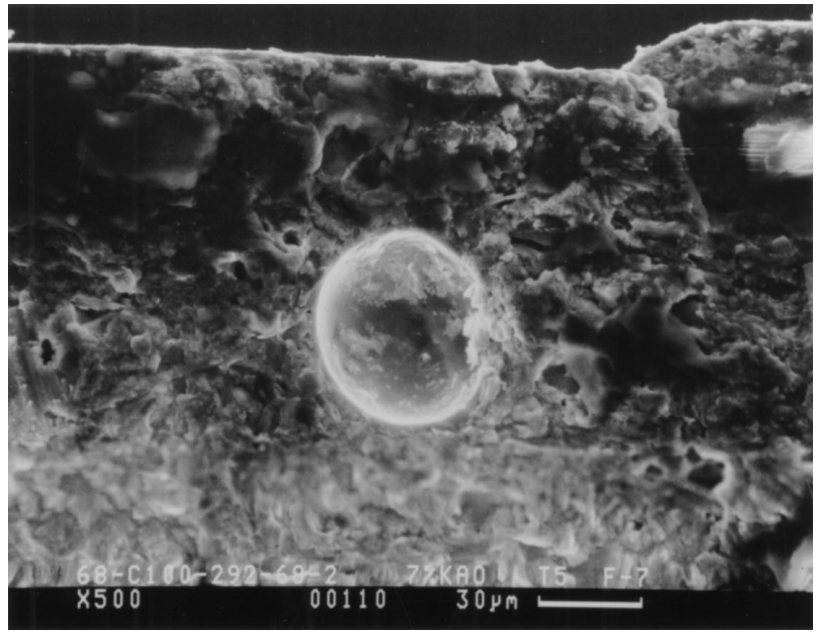

(a)

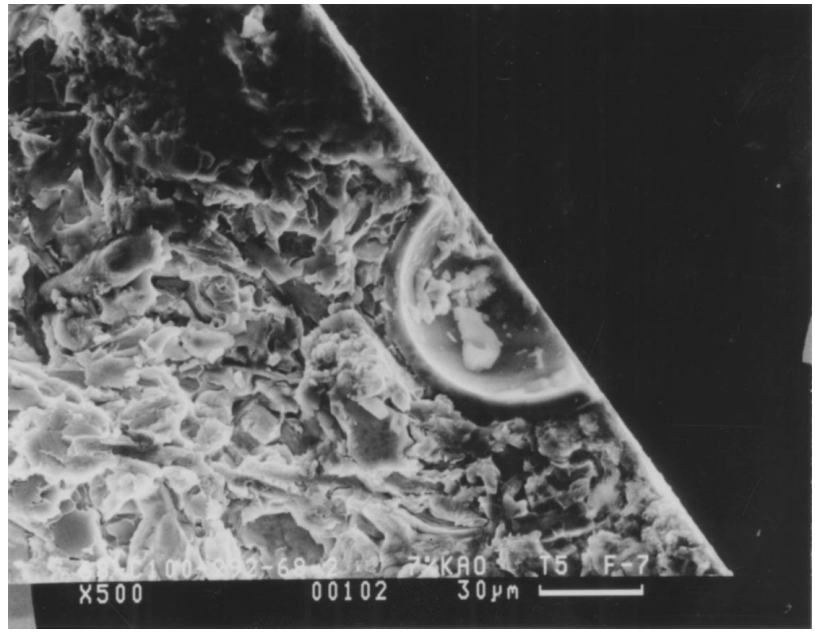

(b)

Figure 17 Scanning electron micrographs of three shot particles on the fracture surface of a specimen of 7% Kaowool/339 aluminum, fatigue tested at ± 124 MPa for 2×10^6 cycles. (a) Particle at fracture origin, (b) and (c) two particles at other locations. The important geometrical parameters and calculated stresses are listed in Table III. *(Continued).*

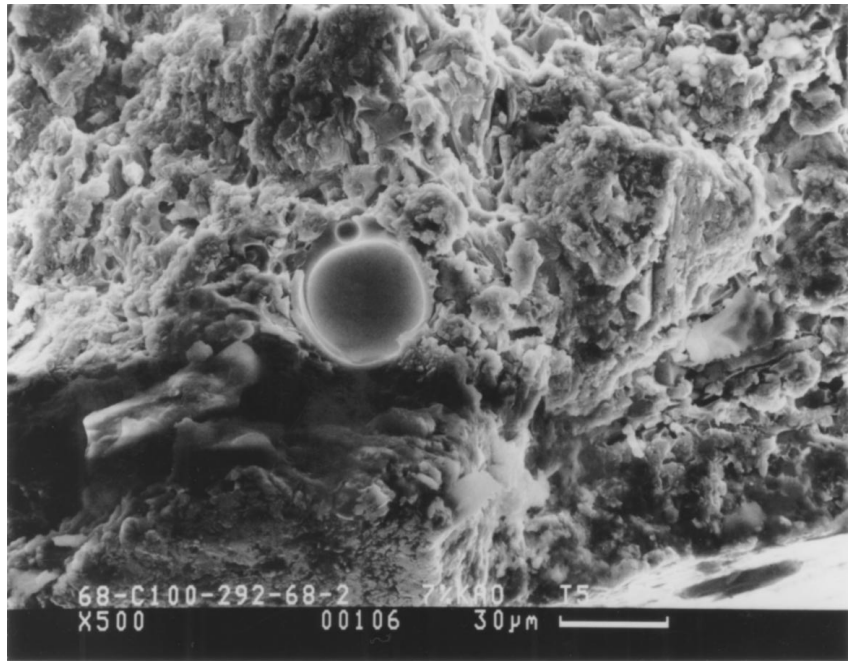

(c)

Figure 17 (Continued).

superimposed on curves relating the calculated stress to the particle wall thickness. Three of these curves show the total stress at D for $d = -a$, 0 and $2a$, while the top curve corresponds to the stress at M for $d = 0$. Note that the four subsurface particles (Figs 17a and c and 18b and c) can all be represented by $d = 2a$ since they all lie in the range where the stress at D is independent of d/a (Fig. 6). A similar plot of the largest stresses in the Kaowool, at either A or C, for each of the six particles is shown in Fig. 20, where the calculated curves represent the total stresses at A for $d = 0$ and $2a$, and at C for $d = -a$. These two graphs provide perspective on the vital role of the geometrical parameters of the shot particles. For the 7% Kaowool specimen the wall thickness was the dominant factor in determining the crack initiation site, whereas for the 15% Kaowool specimen the close proximity to the surface was more important. It is the latter factor which resulted in the shorter fatigue life for the 15% Kaowool specimen.

8. Discussion

During fatigue loading at 20°C the localized stress distribution around shot particles derives from two sources: (i) differential thermal contraction stresses generated as the casting initially cooled down and (ii) the applied cyclic stress. The relative magnitudes of these two components of the localized stress depend upon the wall thickness of the particle. The thermal stresses in the adjacent aluminum matrix are tensile and increase substantially as the wall thickness increases (Fig. 3), whereas the thermal stresses in the Kaowool shell are compressive and decrease slightly as the wall thickness increases (Fig. 4). The mechanically induced stresses in both the matrix and the Kaowool are tensile (under tensile loading) and decrease quite dramatically as the wall thickness increases (Figs 3 and 4). The thermal stresses in the Kaowool are large enough to be beneficial (under tensile loading) and depend only weakly on the wall thickness (Fig. 4) and the distance of the particle from the free surface (Fig. 8). The thermal stresses in the aluminum matrix are deleterious but only significant (i) for subsurface thick walled particles (Fig. 3) and (ii) at location B adjacent to any particle (i.e. all t/a) when near the free surface (Fig. 5). In general, under our applied stress of 120 MPa, the localized mechanically induced stresses are larger than the localized thermal stresses, particularly for the thin walled particles near the surface.

The largest total stresses, both in the aluminum matrix and the Kaowool particle itself, are associated with thin walled particles when at or near a free surface. In this situation the calculated stresses in the matrix can attain the ultimate tensile strength of the 339 aluminum alloy: e.g. this is predicted to occur for $t = 0.05a$ when $d \leq 0.1a$ and for $t = 0.1a$ when $d = 0$ (Figs 12 and 13). Similarly the stress in the shot particle is predicted to exceed the ultimate tensile strength of Kaowool when $d = 0$ and $t \leq 0.2a$ (Fig. 14), or when $t = 0.05a$ and $d \leq 0.6a$ (Fig. 16). If the attainment of the ultimate tensile strength is adopted as a failure criterion, then the upper limits of the combinations of wall thickness and distance from the surface which result in failure are defined by the lines in Fig. 21. On this basis the Kaowool particles are predicted to fracture prior to the aluminum matrix, which may be true in a unidirectional tensile test. However, under the cyclic loading of a fatigue test, the yield strength of the aluminum matrix is a more appropriate failure criterion. The yield strength is 124 MPa, which corresponds to the maximum applied alternating stress required to cause fatigue failure after $\sim 10^6$ cycles. This stress is predicted to be reached at D and M even for subsurface and thick walled particles, the upper limit boundaries for this to occur being as shown in Fig. 21. Thus on this basis, failure is predicted

to initiate preferentially in the aluminum matrix. Further, even thick walled particles are predicted to act as crack initiation sites. At present it is not possible to verify this aspect because all our composites contain shot particles encompassing a wide range of wall thickness, and it is always the thin walled particles which develop the highest stresses and initiate the fatigue failures (Figs 17 and 18).

Since in our model the applied stress P is 120 MPa, this yield stress criterion of 124 MPa is essentially equivalent to the criterion used in our previous study [3], namely that if the local stress is larger than the applied stress the particle is acting as a defect. On this basis our earlier model, which was confined to an elastic analysis at 300°C, predicted that particles remote from the surface would act as defects for wall thicknesses $t \leq 0.28a$. Our elastic analysis at 20°C predicts that all particles will act as defects (Fig. 3), due to the substantial contribution of the thermal stresses for particles with thick walls. However the incorporation of the plasticity of the aluminum matrix renders the model more realistic and reduces the stresses in the aluminum matrix, so that the critical wall thickness for a fully embedded particle to act as a defect is $t = 0.38a$ (Fig. 3), i.e. only marginally thicker than the value of $t = 0.37a$ from the yield stress criterion.

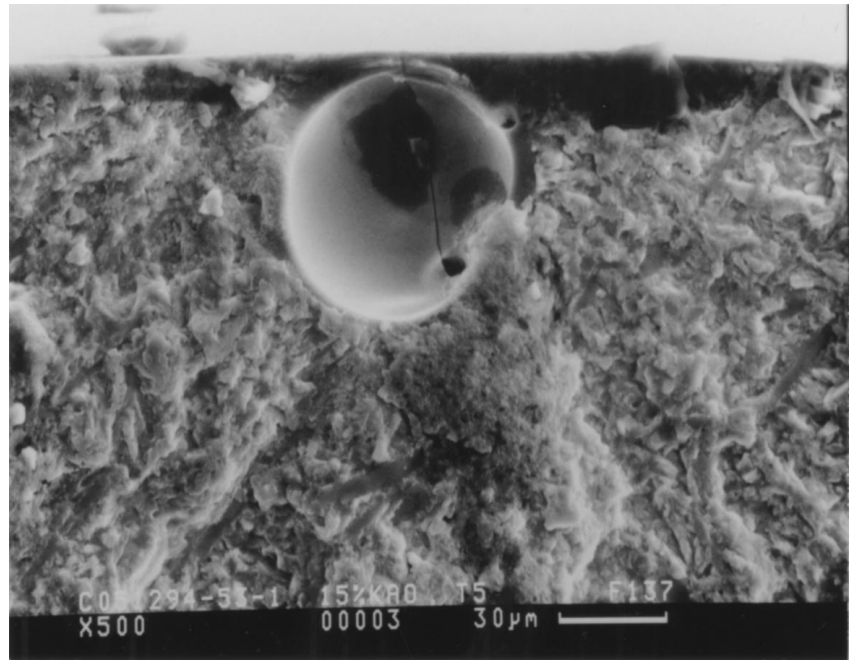

(a)

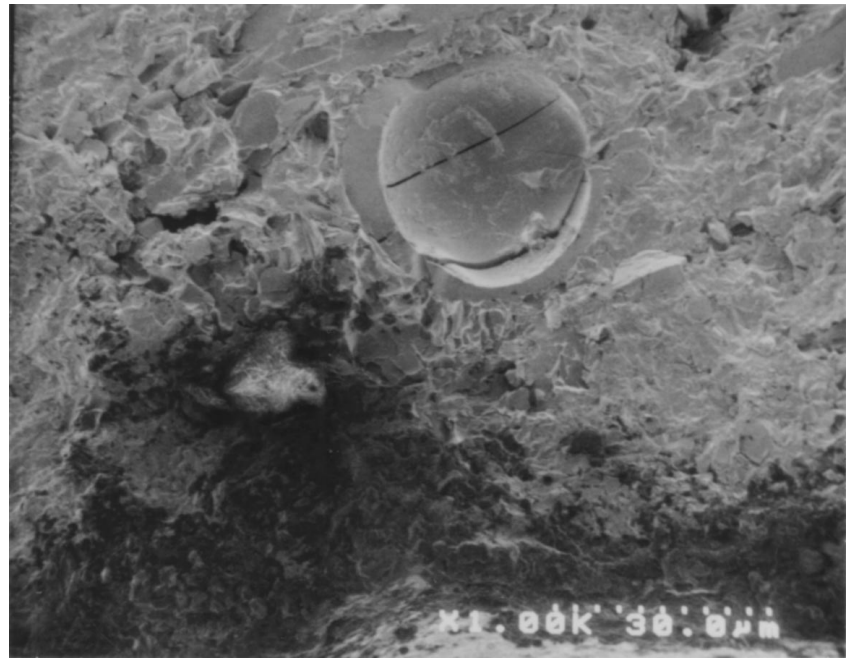

(b)

Figure 18 Scanning electron micrographs of three shot particles on the fracture surface of a specimen of 15% Kaowool/339 aluminum, fatigued at ± 124 MPa for 1.85×10^5 cycles. (a) Particle at fracture origin, (b) and (c) particles at other locations. The important geometrical parameters and calculated stresses are listed in Table IV. *(Continued).*

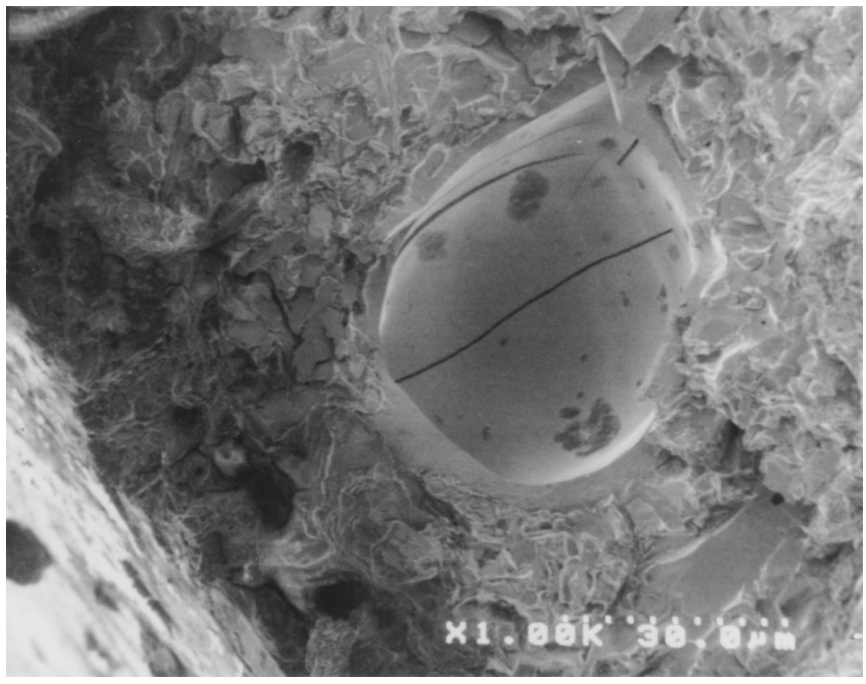

(c)

Figure 18 (Continued).

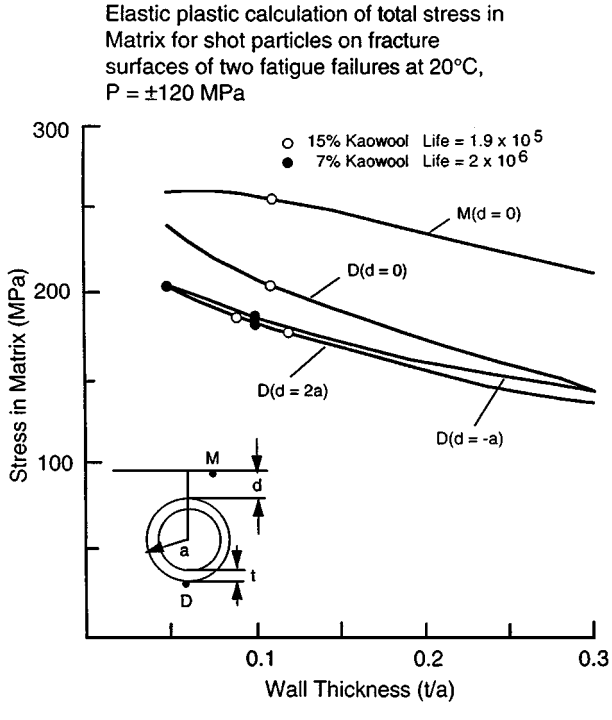

Figure 19 The effect of wall thickness on the total stress in the aluminum matrix at D for particles at $d = 2a$, 0 and $-a$, and at M for $d = 0$. The largest stress associated with each of the shot particles in Figs 17 and 18 is indicated as a data point.

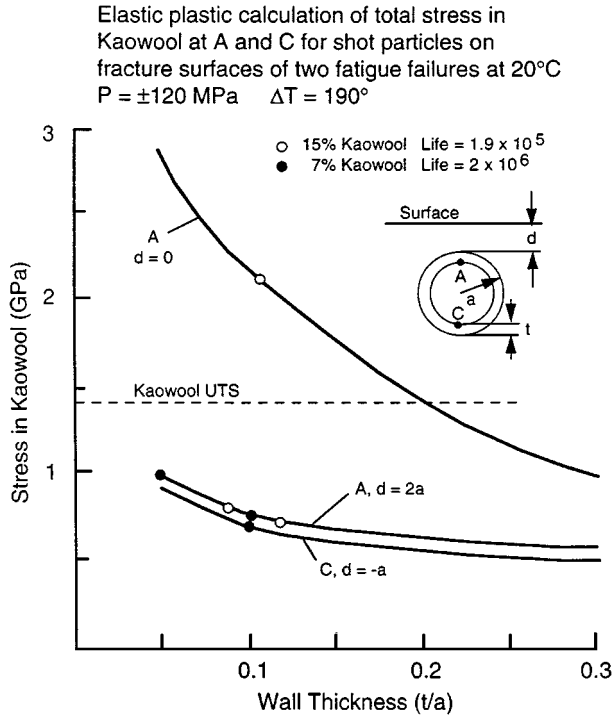

Figure 20 The effect of wall thickness on the total stress in the Kaowool shell at A for particles at $d = 2a$ and 0, and at C for $d = -a$. The largest stress associated with each of the shot particles shown in Figs 17 and 18 is indicated as a data point.

Experimental verification of some of the basic predictions of our finite element model is provided by quantitative comparisons of the calculated stresses with observations of the location and wall thicknesses of the shot particles found on the fracture surfaces of fatigued specimens. It was demonstrated that (i) The dependence of the local stress, in both the aluminum matrix and the Kaowool shell, on the proximity of a thin walled particle to the surface matches the observed locations of the particles causing crack initiation (Figs 15 and 16), (ii) for specimens containing several shot particles, the largest stress in both the aluminum matrix and the Kaowool shell is associated with the particle at the fracture origin (Figs 19 and 20), and (iii) the localized stresses at the fracture origin control the crack initiation rate and thereby the fatigue life of the composite. To elaborate on the last statement, it is interesting to note that the

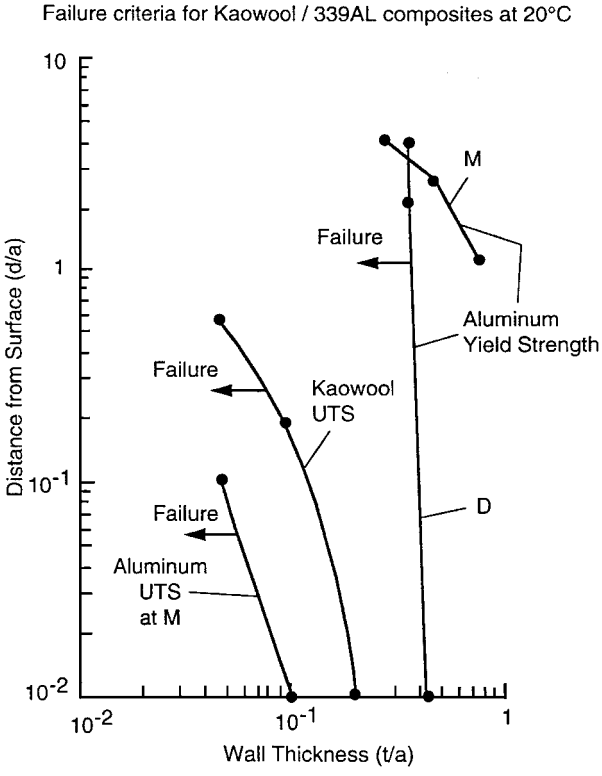

Figure 21 Three failure criteria defined in terms of the combinations of particle wall thickness and the distance of a particle from the free surface. Only particles to the left of each line will initiate fatigue failure by the mechanisms discussed in the text.

specimen with a fatigue life of 1.85×10^5 cycles has a calculated localized stress in the aluminum at M of 255 MPa (Table IV), while the specimen with a fatigue life of 2×10^6 cycles has a calculated stress in the aluminum at D of 204 MPa (Table III). In this regime the relationship between fatigue life (N_f) and the applied cyclic load ($\Delta\sigma$) can be expressed by the empirical Basquin law

$$\Delta\sigma = AN_f^{-b}$$

Substitution of the above values of N_f and $\Delta\sigma$ yields $b = 0.09$, i.e. $N_f \sim (\Delta\sigma)^{11}$. This extremely strong stress dependence is typical for aluminum alloys.

The development of plasticity in the aluminum matrix plays an important role in transferring stress to the Kaowool (Fig. 4) and reducing or limiting the stress in the matrix (Fig. 3). It also accentuates an unexpected effect, namely as a particle approaches the surface, the stress at B decreases while large tensile stresses develop nearby on the free surface at M (Fig. 5). This behavior is attributed to the development of asymmetry in the plastic zone around the particle as it approaches the surface. When the diameter of the plastic zone around the particle is larger than its distance (d) from the surface, more plastic deformation occurs beneath the particle near D than above the particle near B. This results in a hinging action with compression of the matrix at B and tensile deformation of the adjacent material at M. Consequently, the stresses at B and M are sensitive to the choice of the stress-strain relationship used to represent the deformation of the matrix. Our selection of the measured stress-strain curve for the unreinforced alloy (Fig. 2) is reasonable, and the best available. However, if the localized region of the matrix adjacent to the shot particle has a higher yield stress or work hardening rate than the macroscopic value, the stresses at M are reduced, and those at B do not decrease as much. Thus the magnitude of the calculated stresses at M should be viewed with caution.

This hinging action, associated with an asymmetrical plastic zone around a particle adjacent to the surface, may also be accentuated by our 2D representation of a 3D system. In a 2D model the particle and plastic zone are cylindrical, so that interception with the surface removes a continuous segment of the plastic zone. For a spherical particle and plastic zone, interception with the surface only eliminates a cap from the plastic zone. Thus the asymmetry and the hinge action will be smaller in 3D than 2D, and tensile stresses at M will not be as large. A 3D finite element model is being developed to determine the magnitude of this deficiency of our simple 2D representation.

9. Conclusions

1. Under conditions of high cycle fatigue at 20°C, the localized mechanical stresses associated with shot particles are considerably larger than the thermal stresses.

2. As the wall thickness of a shot particle decreases the thermal stress in the aluminum matrix decreases, whereas the larger mechanical, and consequently the total localized stress, increases.

3. Both the thermal and the mechanical stresses in the Kaowool particle decrease as the wall thickness of the particle decreases.

4. As the particle approaches the surface the localized stresses in both the aluminum matrix and the Kaowool shell increase. This effect is more pronounced for thin walled particles.

5. The stresses in the aluminum matrix are more critical than those in the Kaowool particle. When a particle is at the surface, the localized stress in the matrix is predicted to exceed the yield strength of 339 aluminum for all values of wall thickness (t), and to attain the ultimate tensile strength if $t \leq 0.1$ of the particle radius.

6. The shot particles found at the fatigue crack origins are thin walled and usually close to the surface. These observations are in quantitative agreement with the predictions of the finite element model.

Acknowledgments

The authors are grateful to S. M. Willett for performing the fatigue tests, to R. C. Lints for the scanning electron micrographs of the shot particles, and to D. Gerard and D. Meyers of GM Powertrain for supporting the work at Michigan State University.

References

1. Thermal Ceramics, Inc., Augusta, GA.
2. W. J. BAXTER and A. K. SACHDEV, *Metall. and Mater. Trans. A* **30A** (1999) 815.
3. W. J. BAXTER, A. AL-OSTAZ and I. M. JASIUK, *ibid.* **30A** (1999) 195.
4. *Idem.*, "Fatigue of Kaowool Reinforced Aluminum: Effect of Shot Particle Wall Thickness," in preparation.

Received 6 March
and accepted 14 August 2000